Summary

This study has revealed dramatic differences in the binding of arsenite to oxidized and reduced forms of active xanthine oxidase. The additional As-S bond(s) observed under reduced conditions helps to explain the stronger arsenic binding to the reduced forms of the enzyme. However, the information from EXAFS raises new questions about the nature of arsenite binding. For example, it is not known what protein functional groups are involved in the binding of arsenite to the oxidized enzyme. Another important question is whether the thiolate-like sulfurs which bind molybdenum can also interact with inhibitors such as arsenite and mercury. Furthermore, there probably are additional ligands to molybdenum which still have not been identified.

Additional work is necessary to see if Mo-Br and As-Br interactions in the 8-bromoxanthine-complexed material can ever be observed. In this regard, complementary experiments using Br EXAFS are required. Since a number of substrates and inhibitors still bind to the enzyme after arsenite inhibition, it may be possible to study the structure of such complexes from both molybdenum and arsenic points of view. Triangulation using dual or multicenter EXAFS should eventually yield geometric information unavailable from the study of a single absorption edge.

Acknowledgment. We thank the staff of SSRL for their assistance in making this work possible. SSRL is supported by the Department of Energy, Office of Basic Energy Science, and the National Institute of Health, Biotechnology Resource Program, Division of Research Resources.

Registry No. As, 7440-38-2; Mo, 7439-98-7; S, 7704-34-9; O_2, 7782-44-7; arsenite, 15502-74-6; xanthine oxidase, 9002-17-9; 8-bromoxanthine, 10357-68-3.

Supplementary Material Available: Parametrized Mo-X and As-X phase shift and amplitude functions used in the curve-fitting analysis (1 page). Ordering information is given on any current masthead page.

Activation of Methane by Photoexcited Copper Atoms and the Photochemistry of Methylcopper Hydride in Solid Methane Matrices†

J. Mark Parnis, Steven A. Mitchell,‡ Jaime García-Prieto, and Geoffrey A. Ozin*

Contribution from the Department of Chemistry, University of Toronto, Toronto, Ontario, Canada M5S 1A1. *Received July 8, 1985*

Abstract: Photolysis of copper atoms at the 305-325-nm $^2P \leftarrow {}^2S$ resonance absorption in methane matrices at 12 K results in the formation of methylcopper hydride, CH_3CuH, which is characterized by a combination of IR, UV-vis, and ESR spectroscopy and ^1H, ^2H, and ^{13}C isotope-labeling experiments. CH_3CuH is found to be sensitive to tail-end photolysis in a broad absorption band centered at 350 nm and extending into the 305-325-nm Cu atom region. Narrow band photolysis at 350 nm is shown to cause fragmentation of CH_3CuH into CH_3, H, Cu, CH_3Cu, and CuH. In contrast, 10-30 K thermal annealing of matrices containing these fragments results in the reconstitution of CH_3CuH. A mechanism involving a two-step reaction is proposed and supported by experimental evidence as well as by computer simulation of the growth and decay behavior of Cu, CH_3, and CH_3CuH as observed in ESR spectra. The types of electronic and bonding interactions which are thought to be important in the initial C-H bond insertion step are briefly discussed. The molecular structure and bonding in CH_3CuH is considered in light of the experimental observations and recent theoretical proposals.

The activation of C-H bonds of saturated hydrocarbons by metal atoms and metal clusters has been the subject of extensive and diverse research in recent years.[1] The scope of this work encompasses reactions between alkanes and organometallic species in solution,[2] gas-phase atoms[3] and ions,[4] matrix-isolated atoms,[5] supported and unsupported heterogeneous metal and metal oxide catalysts,[6] and metal surfaces.[7] These areas may be further categorized into thermally and photolytically activated processes.

Although the experimental methodologies differ significantly between these fields, similar problems are encountered when attempting to elucidate mechanistic detail associated with the existence of short-lived, thermally and/or photolytically unstable reactive intermediates and products. Often species identification and structure determination is achieved through inference, based upon observed fragments or isotope exchange and labeling studies. The isolation and characterization of reactive intermediates remains one of the major goals sought in the field of C-H bond activation.

† In this paper the periodic group notation is in accord with recent actions by IUPAC and ACS nomenclature committees. A and B notation is eliminated because of wide confusion. Groups IA and IIA become groups 1 and 2. The d-transition elements comprise groups 3 through 12, and the p-block elements comprise groups 13 through 18. (Note that the former Roman number designation is preserved in the last digit of the new numbering: e.g., III → 3 and 13.)

‡ Present address: National Research Council of Canada, Ottawa, Ontario, Canada K1A 0R5.

(1) Muetterties, E. L. *Chem. Soc. Rev.* **1982**, *11*, 283-320.

(2) Parshall, G. W. *Acc. Chem. Res.* **1975**, *8*, 113. Fisher, B. J.; Eisenberg, R. *Organometallics* **1983**, *2*, 764-767. Janowicz, A. H.; Bergman, R. G. *J. Am. Chem. Soc.* **1983**, *105*, 3929-3939. Janowicz, A. H.; Periana, R. A.; Buchanan, J. M.; Kovac, C. A.; Stryker, J. M.; Wax, M. J.; Bergman, R. G. *Pure Appl. Chem.* **1984**, *56*, 13-23. Crabtree, R. H.; Mellea, M. F.; Mihelcic, J. M.; Quirk, J. M. *J. Am. Chem. Soc.* **1982**, *104*, 107-113. Hoyano, J. K.; McMaster, A. D.; Graham, W. A. G. *J. Am. Chem. Soc.* **1983**, *105*, 7190-7191. Rest, A. J.; Whitwell, I.; Graham, W. A. G.; Hoyano, J. K.; McMaster, A. D. *J. Chem. Soc., Chem. Commun.* **1984**, 624-626. Watson, P. L. *J. Am. Chem. Soc.* **1983**, *105*, 6491-6493. Jones, W. D.; Feher, F. J. *J. Am. Chem. Soc.* **1984**, *106*, 1650-1663. Bandy, J. A.; Cloke, F. G. N.; Green, M. L. H.; O'Hare, D.; Prout, K. *J. Chem. Soc., Chem. Commun.* **1984**, 240-242 and references cited therein.

(3) Breckenridge, W. H.; Umemoto, H. In "Dynamics of The Excited State"; Lawley, K. P., Ed.; Wiley: New York, 1982.

(4) Halle, L. F.; Houriet, R.; Kappes, M. M.; Staley, R. H.; Beauchamp, J. L. *J. Am. Chem. Soc.* **1982**, *104*, 6293-6297. Armentrout, P. B.; Halle, L. F.; Beauchamp, J. L. *J. Am. Chem. Soc.* **1981**, *103*, 6624-6628. Jacobson, D. B.; Freiser, B. S. *J. Am. Chem. Soc.* **1983**, *105*, 736-742 and references cited therein.

(5) Ozin, G. A.; Parnis, J. M.; Mitchell, S. A.; García-Prieto, J. In "Chemistry for the Future"; Grunewald, H., Ed.; Pergamon Press: New York, 1984; pp 99-105. Perutz, R. N. *Chem. Rev.* **1985**, *85*, 77-96 and references cited therein.

0002-7863/85/1507-8169$01.50/0

In this paper, details of the photoprocesses of methane-entrapped Cu atoms are reported together with a comprehensive investigation of the spectroscopy and matrix photochemistry of CH_3CuH. The latter represents the first reported organometallic complex of methane and was the subject of two independent communications from the groups of Margrave[8] and Ozin.[9] Subsequently, a number of related systems have been investigated. These include the photochemical reaction of Fe,[10] Mn,[11] Mg,[12a] and Al[12b] atoms with methane, Mg,[12a] Cu,[13] Fe,[14] and Mn[15] atoms with H_2/rare gas matrices, reports on the reactivity of Cu[16] and Fe[17] atoms with ethane and Fe with propane and cyclopropane[17] at 12 K. The previously reported reaction between matrix-isolated Al atoms and methane without photolysis at 12 K[12c] is now known to be incorrect.[12b]

The following investigation of the matrix photochemistry of Cu/CH_4 and CH_3CuH represents the most fully developed matrix-isolation study of an alkane activation system presented to date. Our preliminary studies of the reaction of photoexcited copper atoms with methane can be found in ref 18 as well as in the original communication.[9]

Experimental Section

Monatomic copper atoms were generated by directly heating a tantalum filament around the center of which was wound 0.010 in. diameter copper wire (99.999%, supplied by A. D. McKay, New York). Ultrahigh purity methane gas (99.97%) was supplied by Matheson of Canada. The rate of copper atom deposition was continuously monitored by means of a quartz crystal microbalance built into the furnace assembly.[19] Matrices were deposited on NaCl (UV–visible) or CsI (infrared) optical windows or a sapphire rod (ESR) which were cooled to 12 K by means of an Air Products Displex closed-cycle helium refrigerator. Matrix concentrations were $Cu/CH_4 \cong 1/10^4$ in all cases. UV–visible spectra were recorded on a Unicam SP8000 spectrophotometer in the range of 200–700 nm. Infrared spectra were recorded on a Perkin-Elmer 180 spectrophotometer in the range of 4000–250 cm^{-1}. ESR spectra were recorded on a Varian Model E-4 with a rectangular TE104 cavity at a microwave frequency of approximately 9.3 GHz in the range of 0–6000G. Photolysis at 305–325 nm was carried out by using an Osram XBO 450-W xenon arc lamp in an Oriel Corp. lamp housing equipped with a water-cooled water cell. The lamp output was focussed onto the entrance slit of the monochromator by means of a 10-cm focal length lens. Wavelengths were selected by using either a Schoeffel Model GM 100 or Oriel Model 7240 monochromator with bandwidths of either 20 or 8 nm (fwhm). The lamp power at the sample was approximately 80 μW cm^{-2} for a bandwidth of 20 nm. Photolysis at 350 nm was carried out by using a Corning 7380 UV cutoff filter (330 nm) in addition to the equipment described above. Matrix samples were annealed for periods of 1–30 min between 12 and 40 K, using a 46-Ω foil strip heater attached to the cold tip. In all cases, spectra were recorded after the system had returned to 12 K following annealing.

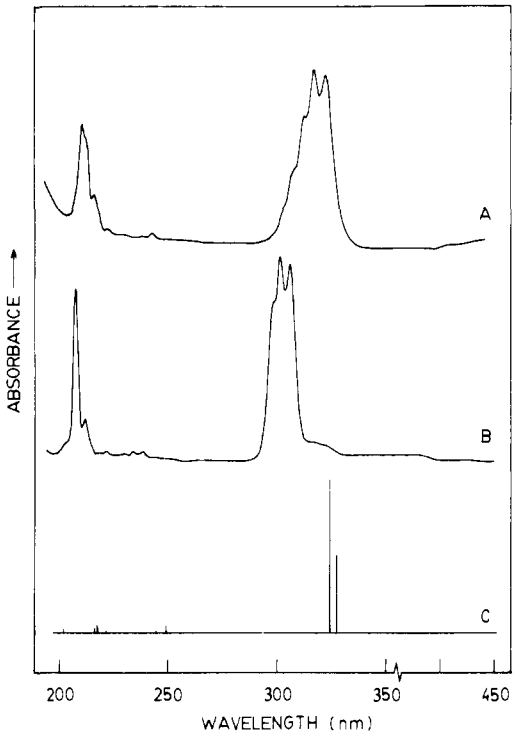

Figure 1. UV–Visible absorption spectra of copper atoms (A) in a methane matrix ($Cu/CH_4 = 1/10^4$, 12 K), (B) in an argon matrix ($Cu/Ar = 1/10^4$, 12 K), and (C) in the gas phase.[20]

Results and Discussion

Primary Photolysis at 305–320 nm. The UV–visible absorption spectrum of copper atoms entrapped in solid methane is shown in Figure 1A. The most prominent spectral feature is the strong absorption at 305–325 nm which can be assigned to the $4p^1$, $^2P \leftarrow 4s^1$, ^2S atomic resonance transition of copper by comparison with the gas-phase copper atom spectra (Figure 1C).[20] The spectrum is similar in appearance to that of copper atoms isolated in rare gas matrices (Figure 1B) except for a difference in the number of observable components in the main absorption. In the case of copper atoms in methane, there are five components of which three (313.0, 317.2, and 322.5 nm) are analogous to the three seen in rare-gas matrix spectra and two (303 and 308 nm) are shown by thermal annealing studies to be due to a secondary trapping site. Similar spectra of Cu atoms isolated in neat methane at liquid helium temperatures have been reported by Abe et al.[21] At this temperature, the high-energy doublet is much more prominent, giving rise to a spectrum in which all five components are of similar intensity. The spectra were interpreted as arising from two sites, and while we agree with the peak positions and number of sites reported, our thermal annealing studies indicate that the two highest-energy peaks are due to copper atoms in a minor site (at 12 K) which is thermally stable with respect to atoms in the site which gives rise to the dominant triplet feature. The splitting of the $^2P \leftarrow {}^2S$ absorption in rare-gas matrices has been the subject of considerable work[22] and will not be further discussed here. For our purpose, it will suffice to say that the three main components show identical growth and decay behavior during thermal annealing and photochemical transformation and are treated in this study as a single band.

It is now well-known that $^2P \leftarrow {}^2S$ excitation of copper atoms in rare gas matrices gives rise to intense $^2D \rightarrow {}^2S$ atomic

(6) Gates, B. C.; Katzer, J. R.; Schmit, G. C. A., "Chemistry of Catalytic Processes"; McGraw-Hill: New York, 1979. Driscoll, D. J.; Martir, W.; Wang, J.-X.; Lunsford, J. H. *J. Am. Chem. Soc.* **1985**, *107*, 58–63. Bhasin, M. M.; Keller, G. E. *Proc. Methane Activat. Chem. Workshop* **1985**, 1.

(7) Somorjai, G. A. "Chemistry in Two Dimensions: Surfaces"; Cornell University Press: Ithica, NY, 1981.

(8) Billups, W. E.; Konarski, M. M.; Hauge, R. H.; Margrave, J. L. *J. Am. Chem. Soc.* **1980**, *102*, 7394–7396.

(9) Ozin, G. A.; McIntosh, D. F.; Mitchell, S. A.; García-Prieto, J. *J. Am. Chem. Soc.* **1981**, *103*, 1574–1575.

(10) Ozin, G. A.; McCaffrey, J. G. *J. Am. Chem. Soc.* **1982**, *104*, 7351–7352.

(11) Ozin, G. A.; McCaffrey, J. G.; McIntosh, D. F. *Pure Appl. Chem.* **1984**, *56*, 111–128.

(12) (a) McCaffrey, J. G.; Parnis, J. M.; Ozin, G. A.; Breckenridge, W. H. *J. Phys. Chem.* **1985**, *89*, 4945. (b) Parnis, J. M.; Ozin, G. A. *J. Am. Chem. Soc.*, submitted. (c) Klabunde, K. J.; Tanaka, Y. *J. Am. Chem. Soc.* **1983**, *105*, 3544–3546.

(13) Ozin, G. A.; García-Prieto, J.; Mitchell, S. A. *Angew. Chem., Int. Ed. Engl. Suppl.* **1982**, 785.

(14) Ozin, G. A.; McCaffrey, J. G. *J. Phys. Chem.* **1984**, *88*, 645.

(15) Ozin, G. A.; McCaffrey, J. G. *J. Am. Chem. Soc.* **1984**, *106*, 807.

(16) Ozin, G. A.; Mitchell, S. A.; García-Prieto, J. *Angew. Chem., Int. Ed. Engl.* **1982**, *21*, 211.

(17) Kafafi, Z. A.; Hauge, R. H.; Fredin, L.; Billups, W. E.; Margrave, J. L. *J. Chem. Soc., Chem. Commun.* **1983**, 1230–1231.

(18) Mitchell, S. Ph.D. Thesis, University of Toronto, 1982.

(19) Moskovits, M.; Ozin, G. A. *Appl. Spectrosc.* **1972**, *26*, 487.

(20) Carstens, D. H. W.; Brashear, W.; Eslinger, D. R.; Gruen, D. M. *Appl. Spectrosc.* **1972**, *26*, 184–217. Moore, C. *Natl. Bur. Stand. (U.S.)* **1958**, *Circ. No. 467*, 1.

(21) Abe, H.; Schulze, W.; Kolb, D. M. *Chem. Phys. Lett.* **1979**, *60*, 208.

(22) Zeringue, K. J.; Emampour, J. S.; Rivoal, J. C.; Vala, M. *Chem. Phys.* **1983**, *78*, 2231. Hormes, J.; Grinter, R.; Breithaupt, B.; Kolb, D. M. *J. Chem. Phys.* **1983**, *78*, 158 and references cited therein.

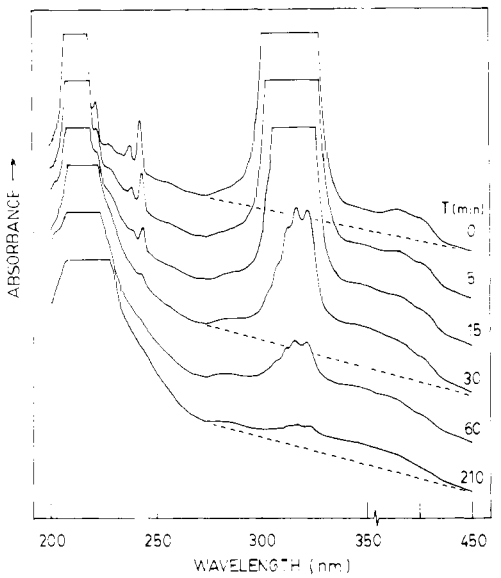

Figure 2. UV–Visible spectra of copper atoms in methane at various points during photolysis at 310 nm (20-nm fwhm). Note the disappearance of features associated with Cu atoms as well as the growth of new features at 350 and 220 nm and the rising base line in the high-energy region (<200 nm).

fluorescence accompanied by photoinduced diffusion and aggregation of copper atoms.[23] This is not the case in methane, where excitation results in rapid loss of copper atomic absorption without any evidence of fluorescence or aggregation. The depletion of copper atoms is accompanied by growth of a broad feature at 220 nm, a gradual rise in the base line near the high-energy limit, indicating an absorption below 200 nm, as well as growth of a very broad absorption centered at 350 nm, as seen in Figure 2. During the course of the photolysis, these new absorptions exhibit two distinct types of behavior, allowing them to be classified as those which continue to grow and persist (220 nm/<200 nm; denoted final products) and those which grow to a maximum value and then diminish until gone (350 nm; denoted intermediate product(s)). The transient nature of this intermediate will be shown to be due to tail-end absorption by the broad 350-nm band, which results in a secondary photochemical conversion of this species to other fragments. It should be noted that while matrix-isolated Cu_2 was present in small amounts in most samples (285, 395, and 410 nm and others), no growth of Cu_2 dimer was observed within detection limits during the entire atomic photolysis (Figure 2). This is to be sharply contrasted with the behavior of copper atoms in rare-gas matrices, wherein significant growth of Cu_2 may be observed after brief photolysis of Cu atoms.[23]

The decay behavior of the atomic absorbance due to copper atoms during 305–325-nm photolysis was found to exhibit a Beer–Lambert law dependence of atom loss on photon flux. The rate of atom depletion was found to be essentially unchanged for photolysis of copper atoms isolated in CD_4 matrices, as well as for photolysis at several temperatures between 12 and 25 K. Analogous behavior was found for copper atom depletion during photolysis as observed by ESR spectroscopy and is discussed in detail below.

The effects of $^2P \leftarrow {}^2S$ electronic excitation of copper atoms in methane were studied by using infrared absorption spectroscopy. Figure 3 illustrates successive scans taken at various stages during a 320-nm photolysis of a typical sample. The frequencies of the observed absorbances associated with products are given with spectral assignments in Table I. Included in this tabulation is the corresponding data for photolysis of copper atoms in CD_4 and $^{13}CH_4$ matrices. As with the UV–visible results, the growth and decay behavior of these new absorbances allows one to group them into those associated with intermediate products (1697 and 1011 cm^{-1}) and those due to final products (1850 and 611 cm^{-1} and others).

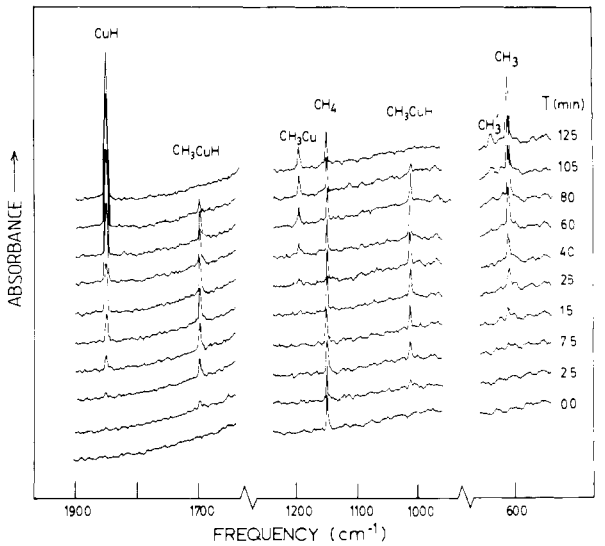

Figure 3. Infrared spectra of a Cu/CH_4 matrix at 12 K, recorded at various stages of photolysis at 320 nm, ranging from 0-min (bottom trace) to 125-min total photolysis time (top trace).

Table I. Infrared Frequencies (cm^{-1}) and Assignments for Copper Atom–Methane Photoproducts in CH_4, CD_4, and $^{13}CH_4$ Matrices at 12 K[a]

CH_4	CD_4	$^{13}CH_4$		assignment[c,d]
1850 s	1333 s	1850 s	CuH	ν(CuH)
3171 vw	*b*	*b*	CH_3	ν_d(CH)
611 m	463 m	608 m	CH_3	$\pi(CH_3)$
640 vw	493 vw	*b*	CH_3[e]	$\pi(CH_3)$
2929 vw	2108 vw	2920 vw	$CuCH_3$	$\nu(CH_3)=\nu_1(a_1)$
2880 vw	*b*	2880 vw	$CuCH_3$	$\nu_d(CH_3)=\nu_4(e)$
1344 w	1012 w	1339 w	$CuCH_3$	$\delta_d(CH_3)=\nu_5(e)$[f]
1328 w	1009 w	1322 w	$CuCH_3$	
1196 w	916 w	1189 w	$CuCH_3$	$\delta_s(CH_3)=\nu_2(a_1)$
433 m	316 m	433 m	$CuCH_3$	$\rho_r(CH_3)=\nu_6(e)$[f]
414 m	305 w	416 m	$CuCH_3$	
351 m	260 m	350 m	$CuCH_3$	ν(CuC)=$\nu_3(a_1)$
1697 w	1229 w	1697 w	$HCuCH_3$	ν(CuH)
1011 w	786 w	1003 w	$HCuCH_3$	$\delta_s(CH_3)$

[a] s denotes strong bands, m medium bands, w weak bands, and vw very weak bands. [b] Bands too weak to observe or obscured by strong matrix absorptions. [c] Assignments refer to the case of a $^{12}CH_4$ matrix. The appropriate isotopic counterparts apply for $^{12}CD_4$ and $^{13}CH_4$ matrices. [d] The descriptive symbols have the following meanings: ν_d, degenerate stretch; ν, nondegenerate stretch; π, out-of-plane bend; δ_d, degenerate deformation; δ_s symmetric deformation; ρ_r, rocking mode. [e] Assignment refers to CH_3 subject to a matrix perturbation. [f] Appearance of pairs of absorptions attributed to removal of the degeneracy of the vibrational mode by a matrix perturbation.

The two most prominent bands in the spectra are those at 1850 and 611 cm^{-1}, both of which are attributed to final products. The 1850-cm^{-1} band was found to shift to 1333 cm^{-1} in a CD_4 matrix and was unshifted in a $^{13}CH_4$ matrix. These frequencies are quite close to the gas-phase values for CuH and CuD (1866 and 1346 cm^{-1}, respectively),[24] and the observed frequency ratio of 1.388 is very similar to the gas-phase value of 1.386. When experiments were carried out in mixed CH_4/CD_4 matrices or CH_nD_{4-n} (n = 1–3) matrices, both the 1850- and 1333-cm^{-1} bands appeared without any new absorbances attributable to a CuHD dihydride species. It is clear that the 1850-cm^{-1} band is due to CuH. The broad UV–visible absorbance at 220 nm is most likely associated with the D $\leftarrow$ X system of CuH, for which the 0–0 transition occurs in the gas phase at 222 nm.[24] Experiments involving H/D

(23) Ozin, G. A.; Mitchell, S. A.; García-Prieto, J. *J. Phys. Chem.* **1982**, *86*, 473–479.

(24) Huber, K. P.; Herzberg, C. "Molecular Spectra And Molecular Structure. IV Constants of Diatomic Molecules"; Van Nostrand Reinhold: New York, 1979.

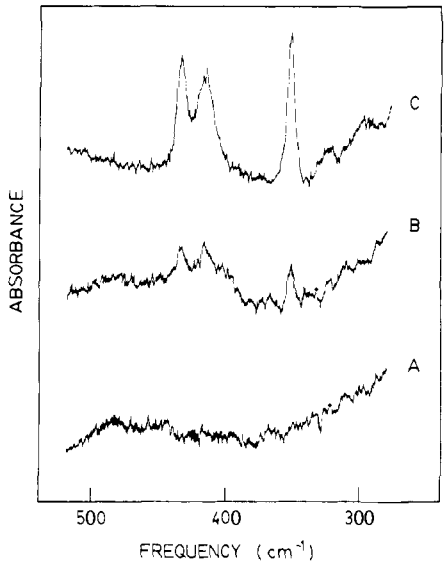

Figure 4. Infrared spectra of a Cu/CH_4 matrix in the low-energy region (A) before photolysis, (B) brief photolysis, and (C) after extensive photolysis at 320 nm. The three peaks at 433, 414, and 351 cm^{-1} are associated with the final product, $CuCH_3$.

and $^{12}C/^{13}C$ isotopic substitution yielded data for the 611-cm^{-1} IR band which was found to be in excellent agreement with the results of Milligan and Jacox[25] for isotopic CH_3 molecules trapped in solid nitrogen at 14 K. On the basis of these results, the 611-cm^{-1} absorbance can be attributed to isolated methyl radicals, which are most likely responsible for the rising base line (<200 nm) observed in the UV–visible spectra.[25] This assignment receives strong support from the observation of intense features in the ESR spectra of Cu atoms in methane after 320-nm photolysis characteristic of methyl radicals as described below.

The growth and decay patterns for all product IR absorbances during photolysis indicate that there are at least two distinct products other than methyl radicals and CuH involved in this reaction. The band at 1196 cm^{-1}, associated with a final product in CH_4, was found to shift to 916 cm^{-1} in a CD_4 matrix and 1189 cm^{-1} in a $^{13}CH_4$ matrix. These frequencies are characteristic of a symmetric bending vibration of a coordinated methyl group. Absorbances due to this type of mode have been reported by Andrews[26] for matrix-isolated methyllithium monomers, appearing at 1158 cm^{-1} for $LiCH_3$, 886 cm^{-1} for $LiCD_3$, and 1152 cm^{-1} for $Li^{13}CH_3$. The H/D and $^{12}C/^{13}C$ ratios for methyllithium are 1.307 and 1.005, respectively, compared with 1.306 and 1.006 for this species. This, along with the fact that the 1196-cm^{-1} band exhibits four degrees of deuterium isotope substitution in experiments involving CH_nD_{4-n} (n = 0–4) matrices (bands at 1058-cm^{-1} CH_2D, 960-cm^{-1} CHD_2, and 916-cm^{-1} CD_3), strongly supports the identification of this species as the methylcopper monomer, $CuCH_3$. Also associated with the 1196-cm^{-1} band are three bands at 433, 414, and 351 cm^{-1} (Figure 4) which show similar growth and decay behavior. The pair at 433 and 414 cm^{-1} are assigned, by comparison to $LiCH_3$, to the doubly degenerate (e) rocking mode of CH_3 in which the degeneracy has been lifted due to a matrix cage perturbation effect. The band at 351 cm^{-1} is tentatively assigned to the C–Cu stretching mode. These proposals receive strong support from the results of a complete normal coordination analysis[27] of $CuCH_3$ (with isotope substitution). The calculated and observed frequencies for $CuCH_3$ are listed in Table II and are found to be in quite close agreement, thereby supporting the vibrational assignments and the identification of this species as $CuCH_3$.

Table II. Normal Coordinate Analysis for $CuCH_3$, $CuCD_3$, and $Cu^{13}CH_3$[a]

$Cu^{12}CH_3$		$CuCD_3$		$Cu^{13}CH_3$		vibrational assignment
calcd	obsd	calcd	obsd	calcd	obsd	
2926	2929	2108	2108	2922	2920	a_1, $\nu(CH_3)$
2883	2880	2087		2877	2880	e, $\nu(CH_3)$
1329	1336	1011	1011	1329	1331	e, $\delta_d(CH_3)$
1201	1196	941		1183	1189	a_1, $\delta_s(CH_3)$
421	424	330	310	417	426	e, $\rho_r(CH_3)$
345	350	290	260	339	350	a_1, $\nu(CuC)$

[a] Root mean square error in eigenvalues, 11.6 cm^{-1}. ν(Cu–C) force constant, 1.75 mdyne $Å^{-1}$. ν(C–H) force constant, 4.57 mdyne $Å^{-1}$.

The band at 1697 cm^{-1}, associated with an intermediate, shifted to 1229 cm^{-1} in a CD_4 matrix and was unshifted in a $^{13}CH_4$ matrix. The H/D ratio for this band is 1.381, which may be compared with the value of 1.388 for CuH/CuD. This band is therefore most likely attributable to a copper–hydrogen stretching mode of a CuH-containing species. Since there was no evidence for a dihydride species in any of the mixed matrix experiments (CH_4/CD_4 or CH_nD_{4-n} (n = 1–3)), this species is most likely a monohydride. The band at 1011 cm^{-1} which showed behavior similar to that of the 1697-cm^{-1} band shifted to 786 cm^{-1} in a CD_4 matrix and 1003 cm^{-1} in $^{13}CH_4$. As with $CuCH_3$, this band exhibited four degrees of deuterium isotope substitution (1011-cm^{-1} CH_3, 947-cm^{-1} CH_2D, 860-cm^{-1} CHD_2, and 786-cm^{-1} CD_3). These frequencies are again suggestive of a symmetric bending vibration of a methyl group, similar to that of $CuCH_3$ discussed above. The H/D and $^{12}C/^{13}C$ ratios for the 1011-cm^{-1} band are 1.286 and 1.008, respectively, which may be compared with 1.306 and 1.006 for $CuCH_3$. Based on these facts, this intermediate is identified as methylcopper hydride, CH_3CuH, a conclusion which is supported by the thermal annealing and secondary photolysis behavior of this species, to be discussed below. Note also that the broad absorption centered at 350 nm, associated with an intermediate product in the UV–visible of Cu atoms photolyzed at 320 nm in methane, is ascribed to CH_3CuH, its behavior being analogous to that of the 1697- and 1011-cm^{-1} IR bands during both primary 320-nm and secondary 350-nm photolysis as well as during thermal annealing.

A typical ESR spectrum of freshly deposited copper atoms isolated in a methane matrix at 12 K is shown in Figure 5. The spectrum is very similar to that of Cu atoms trapped in Kr matrices, as reported by Kasai and McLeod.[28] Evaluation of the hyperfine coupling constant A and the g value for ^{63}Cu in solid methane according to the analysis described by Kasai and McLeod yielded values of A = 5998 MHz and g = 2.004, which are close to the values of A = 6043 MHz and g = 1.995 for ^{63}Cu in krypton matrices. Photoexcitation of copper atoms in methane matrices at 320 nm caused rapid depletion of the ESR lines associated with atomic copper, while giving rise to intense features associated with matrix-isolated methyl radicals and hydrogen atoms[29] (Figure 6). Spectral features due to CD_3 radicals and deuterium atoms were observed after photolysis of copper atoms in CD_4 matrices. A comparison of the total peak-to-peak height for the methyl radicals and hydrogen atoms indicates that for impurity-free samples, methyl radicals are the major ESR-active product, with typical peak height ratios of $\cong$ 80:1 (CH_3:H).[30] This ratio was found to be extremely sensitive to matrix impurities. For example, samples which showed significant amounts of copper dioxygen

(25) Milligan, D. G.; Jacox, M. E. *J. Chem. Phys.* **1967**, *47*, 5146–5156.
(26) Andrews, L. *J. Chem. Phys.* **1967**, *47*, 4834–4842.
(27) McIntosh, D. F.; Peterson, M. R. "General Vibrational Analysis Programs Utilizing the Wilson GF Matrix Method for a General Unsymmetrical Molecule"; Indiana University: Bloomington, IN, 1980; Programs No. 342.
(28) Kasai, P. H.; McLeod, D., Jr. *J. Chem. Phys.* **1971**, *55*, 1566 and references cited therein.
(29) Jen, C. K.; Foner, S. W.; Cochran, E. L.; Bowers, V. A. *Phys. Rev.* **1958**, *112*, 1169.
(30) Experimentally, the peak-to-peak width and line shape of the ESR resonances associated with CH_3 and H were found to be essentially the same. Under these circumstances, it is justifiable to measure the relative concentration of CH_3 to H by means of the experimentally observed peak-to-peak amplitude. See: "Electron Spin Resonance: Elementary and Theory and Practical Application"; Bolton, J. R., Wertz, J. G., McGraw-Hill: New York, 1972.

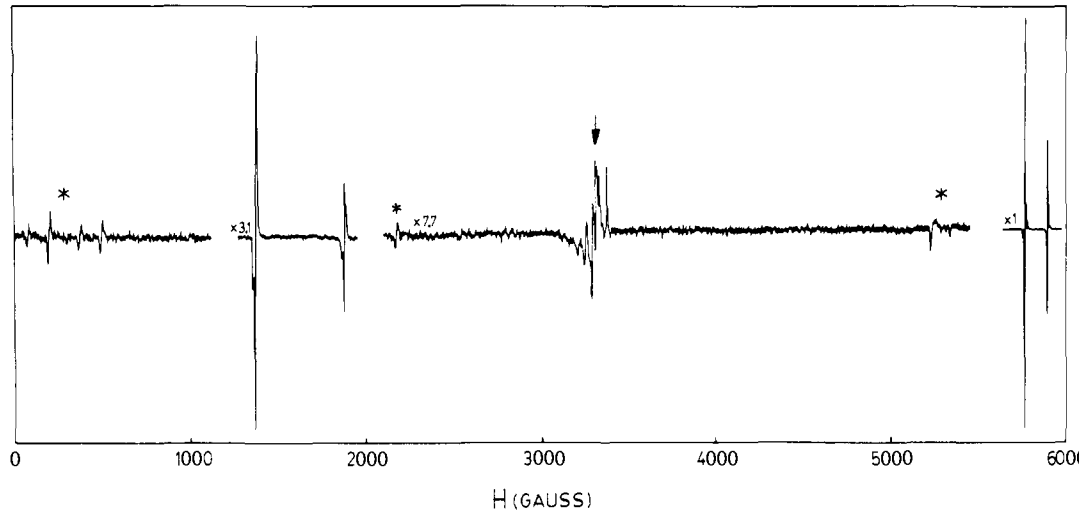

Figure 5. ESR spectrum of Cu atoms isolated in methane between 0 and 6000 G. Minor features associated with $Cu(O_2)$ species are indicated with an arrow. Absorbances due to an unidentified impurity present on deposition are indicated with an asterisk.

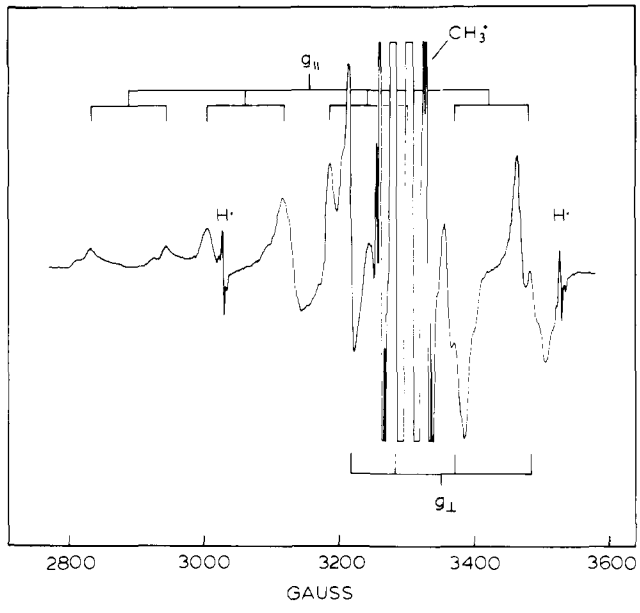

Figure 6. ESR spectrum of the 2800–3600-G region of a Cu/CH_4 matrix after partial photolysis at 315 nm (20 min, 8-nm fwhm). All features are associated with the intermediate product CH_3CuH except where indicated. Stick diagrams indicated the position of Cu ($I = {}^3/_2$) hyperfine components associated with $g_{\|}$ and $g_{\perp}$. Superhyperfine splitting due to the ^1H nucleus is indicated for the $g_{\|}$ components.

complexes[31] on deposition (easily visible in the ESR spectra) yielded CH_3/H ratios of 10–25:1. It is likely that in these cases, hydrogen atoms are formed via an oxygen-mediated pathway, possibly associated with the observed depletion of the copper dioxygen complexes during 305–325-nm photolysis.

In addition to the lines associated with CH_3 and H, features were observed between 2800 and 3600 G after brief photolysis at 315 nm (20 min, 8-nm fwhm), as seen in Figure 6. These features were found to exhibit growth and decay behavior similar to the IR and UV–vis bands assigned to CH_3CuH above, being both stable over long periods of time without photolysis and below 40 K and completely annihilated after prolonged photolysis at 305–325 nm. The general appearance of the intermediate absorbance is consistent with that of a randomly oriented axial molecule with $g_{\|} \simeq 2.10$ and $g_{\perp} \simeq 1.98$. Spectra recorded in CH_4, CD_4, and $^{13}CH_4$ exhibit superhyperfine splitting attributable to hydride, deuteride, and carbon-13 nuclei, respectively, which is characteristic of a compound containing both carbon and hydrogen bonded to copper. As well, hyperfine splitting due to an $I = {}^3/_2$ nucleus with intensity ratios corresponding to that of copper isotopes in natural abundance ($^{63}Cu/^{65}Cu = 69/31$) can be detected, indicating the presence of a single copper atom. The ESR data for this species are therefore consistent with the formulation, CH_3CuH. Hyperfine coupling constants for the various isotopically substituted molecules are estimated as $A_{\|}(^1H) = 320$ MHz, $A_{\|}(^2H) = 45$ MHz, $A_{\perp}(^{63}Cu) = 235$ MHz, $A_{\|}(^{63}Cu) = 514$ MHz, and $A(^{13}C) = 100$ MHz. A detailed analysis of the ESR spectrum of CH_3CuH is somewhat hindered by band overlap with strong methyl radical resonances around 3300 G. Therefore, a complete understanding will require an appropriate theoretical analysis of the magnetogyric and hyperfine tensors for CH_3CuH with spectral line-shape simulation.

Thermal Annealing Studies. The effects of thermal annealing (12–35 K) on the IR absorbances of various products present after 315-nm photolysis of copper atoms in methane are illustrated in Figure 7. As in all cases studied, absorptions associated with CuH, CH_3, and CH_3Cu were observed to diminish upon warming, while those associated with CH_3CuH were found to reappear. The observed behavior is indicative of a thermally induced recombination process (CH_3 + CuH and CH_3Cu + H) to form primarily CH_3CuH. Similar behavior can be observed in the UV–visible (see Figure 8) and ESR spectra of photolyzed copper atoms in methane after annealing. At no time was significant growth of any other fragments or species detected after thermal annealing. In most cases, the amount of CH_3CuH recovered through thermal annealing was low with respect to that which would be expected for complete recombination. This presumably reflects the efficiency of a recombination process in which the main reaction competes with several nonproductive routes such as hydrogen, methane, ethane, and copper cluster formation. It is expected that under extremely dilute conditions, the yield of CH_3CuH would be much higher due to a lack of neighboring reactive fragments.

These observations are important for the following reasons. First, the formation of CH_3CuH from fragments formed as a result of photoinduced decomposition indicates that the intermediate is thermodynamically more stable than its fragmentation products. Second, the fact that no copper atom growth is observed during annealing studies indicates that thermally induced reductive elimination from the ground state of CH_3CuH is not a source of copper atoms during 350-nm photolysis of CH_3CuH, to be discussed below.

Secondary Photolysis at 350 nm. From the results and discussion presented above, it is now possible to outline the various reaction pathways which may be associated with $^2P \leftarrow {}^2S$ excitation of copper atoms in methane at 305–325 nm. The three most likely possibilities are illustrated in Figure 9. These are (1)

(31) Ozin, G. A.; Mitchell, S. A.; Garcia-Prieto, J. *J. Am. Chem. Soc.* **1983**, *105*, 6399–6405. Tevault, D. E.; Smardzewski, R. R.; Urban, M. W.; Nakamoto, K. *J. Chem. Phys.* **1982**, *77*, 577.

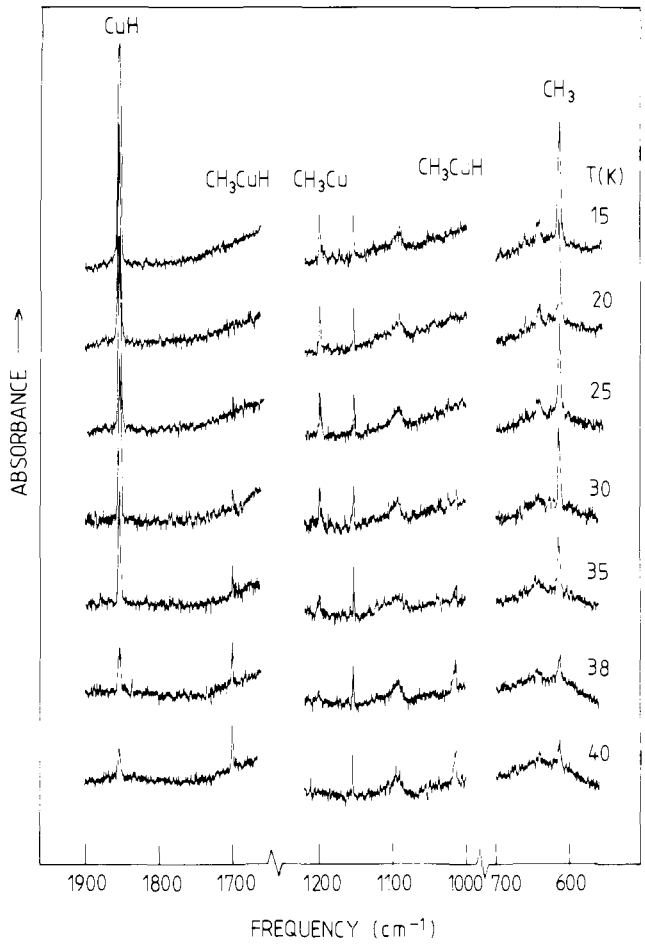

Figure 7. Infrared spectra of a Cu/CH_4 matrix after thermal annealing to various temperatures between 15 and 40 K. In all cases, the sample was brought to the annealing temperature, held for 15 min, and then cooled to 15 K before recording a spectrum. Note the reappearance of features associated with CH_3CuH, along with the loss of absorbances due to CH_3, CuH, and CH_3Cu.

insertion of ^2P copper atoms into the C–H bond of CH_4 to form CH_3CuH, followed by secondary photolysis of CH_3CuH to form all other fragments, (2) abstraction of hydrogen from CH_4 by ^2P copper atoms to form CuH and CH_3 followed by rapid recombination of these fragments to form CH_3CuH which would then be subject to secondary photolysis to give all other fragments, and (3) insertion of ^2P copper atoms into the C–H bond of CH_4 to form CH_3CuH in an unbound or dissociative excited state, followed by fragmentation or relaxation to the ground state of CH_3CuH, itself subject to fragmentation via secondary photolysis. Virtually every fragment which could arise from any of these three mechanisms can be accounted for by using IR and ESR spectroscopy. It is not, however, readily apparent from which pathway the observed fragments arise nor whether their presence can be attributed to a single route.

The three mechanistic pathways presented above invoke one common step after the initial excitation of copper atoms to the ^2P state, namely, the secondary photolysis of the intermediate CH_3CuH from tail-end absorption around 305–325 nm. We have therefore undertaken the study of the photolytic behavior of CH_3CuH in detail in an attempt to shed light on the reaction mechanism.

As mentioned above, the broad absorption centered at 350 nm which is present as an intermediate band in the UV–visible spectrum of partially photolyzed samples of copper atoms in solid methane can be attributed to CH_3CuH. The breadth of this absorption strongly suggests the possibility of tail-end photolysis of this intermediate during 305–325-nm excitation of copper atoms. In order to probe the photolytic properties of this product, photolysis was carried out at 350 nm on samples containing large

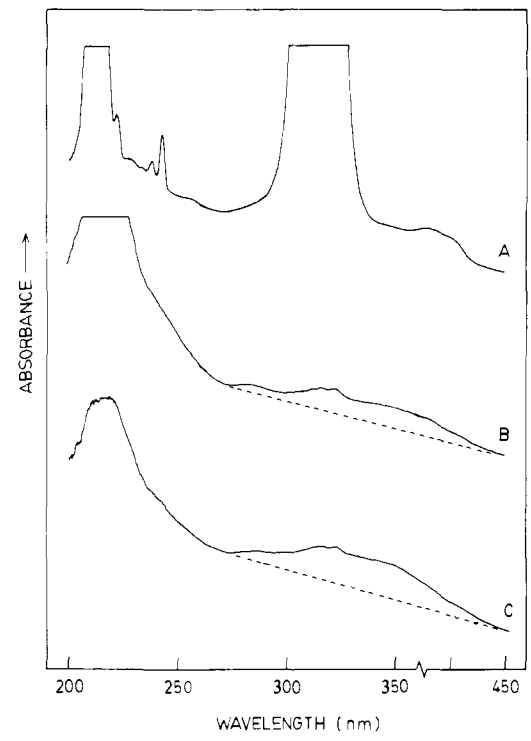

Figure 8. UV–Visible spectra of a Cu/CH_4 matrix (A) on deposition, (B) after extensive photolysis at 310 nm (210 min), and (C) following subsequent annealing to 35 K for 1 h. The reappearance of the broad absorption at 350 nm can be clearly seen along with the loss of absorbances at 220 nm due to CuH.

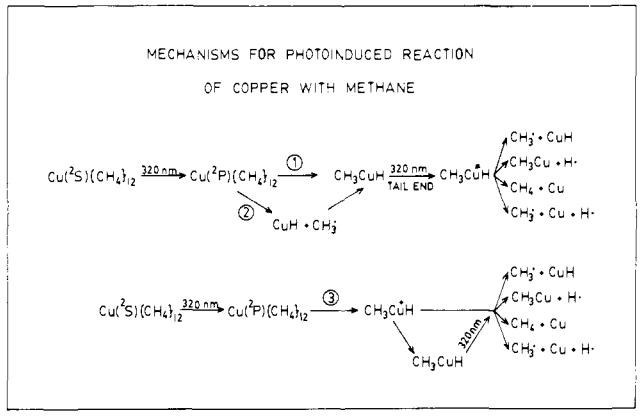

Figure 9. Three possible mechanisms for the photoinduced reaction of copper atoms with methane at 12 K. (1) C–H bond insertion. (2) Hydrogen atom abstraction and fragment recombination. (3) C–H bond insertion to form CH_3CuH in a dissociative excited state.

amounts of CH_3CuH. Such samples were generated by narrow-band (8-nm fwhm) excitation of copper atoms in methane at 305–315 nm. This procedure was found to reduce the secondary photolysis of the intermediate somewhat, resulting in increased concentrations of CH_3CuH after about 30 min of photolysis. In order to ensure that no complications arose from further reaction of copper atoms during 350-nm photolysis, a UV cutoff filter was placed in the beam path. The effects of 350-nm photolysis on CH_3CuH were studied by using a combination of UV–visible, infrared, and ESR spectroscopies, and the results are presented below.

Figure 10 illustrates the effects of 350-nm photolysis on the UV–visible absorption spectrum of partially photolyzed copper atoms in methane (305 nm, 60 min). The most striking changes are the reappearance of significant amounts of copper atoms, typically a recovery of about 20% of the initial absorbance but varying with sample preparation conditions and the extent of bleaching of the 350-nm absorption band. Note the presence of

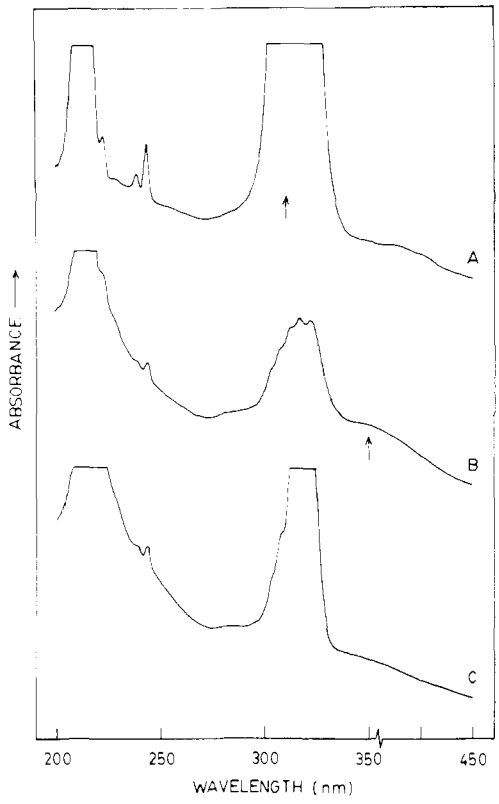

Figure 10. UV–Visible spectra of a Cu/CH_4 matrix (A) after deposition, (B) following partial photolysis at 305 nm (60 min), and (C) following subsequent 350–nm photolysis (45 min). Note the extensive regeneration of copper atoms which accompanies the disappearance of the 350-nm absorption band.

copper dimer absorptions at 375 and 405 nm both before and after photolysis. The previously reported C–H bond activation by Cu_2 in methane during 378-nm photolysis[32] is now believed to be due to the photofragmentation of CH_3CuH, which would be present after 320-nm photolysis of Cu atoms and which absorbs in this region. This conclusion can be readily verified by photolyzing Cu_2-enriched samples at 375 and 405 nm *before* photolysis of the copper atoms at 320 nm. In this case, extremely small amounts of methyl radicals and hydrogen atoms can be detected as products in the ESR spectrum. Such concentrations of ESR active radicals can, however, be produced by photolysis of trace amounts of $Cu(O_2)$ sometimes present in the matrix on deposition. It is therefore likely that these fragments find their origin in this extraneous process.

ESR spectra of partially photolyzed Cu atoms in methane (305 nm, 70 min) were studied before and after photolysis at 350 nm (20-nm fwhm). This photolysis resulted in the complete disappearance of all features associated with CH_3CuH accompanied by growth of the absorbances due to copper atoms, methyl radicals, and hydrogen atoms. Typical growth of Cu atoms accounted for 15% of the atoms present on deposition, using a peak height comparison. Note that this represents a significant recovery of Cu atoms due to the fact that the amount of CH_3CuH present at the time of 350-nm photolysis never exceeds 65% of its theoretical yield due to its subsequent fragmentation to form final products. (In all cases studied, at least 35% of the CH_3 fragments formed as final products were present at the time of 350-nm photolysis.) Thus, a 15% recovery of Cu atoms represents an actual yield of about 25% when "normalized" with respect to the amount of CH_3CuH present at the time of photolysis. This pathway is therefore a significant fragmentation route. The peak height ratio for CH_3/H remained constant after 350-nm photolysis, which suggests that the process which gives rise to the product

(32) Ozin, G. A.; Mitchell, S. A.; Garcia-Prieto, J. *Angew. Chem. Suppl.*, **1982**, 798–806.

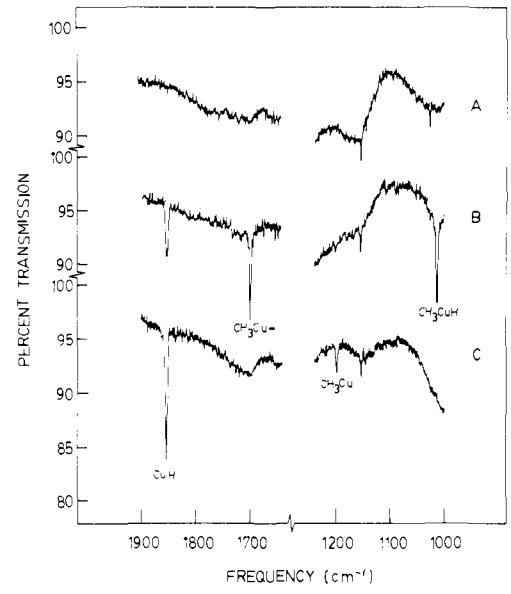

Figure 11. Infrared spectra of a Cu/CH_4 matrix (A) on deposition, (B) after partial photolysis at 315 nm (30 min), and (C) after subsequent photolysis at 350 nm (90 min). Note the growth of CuH and CH_3Cu absorbances and the disappearance of CH_3CuH bands.

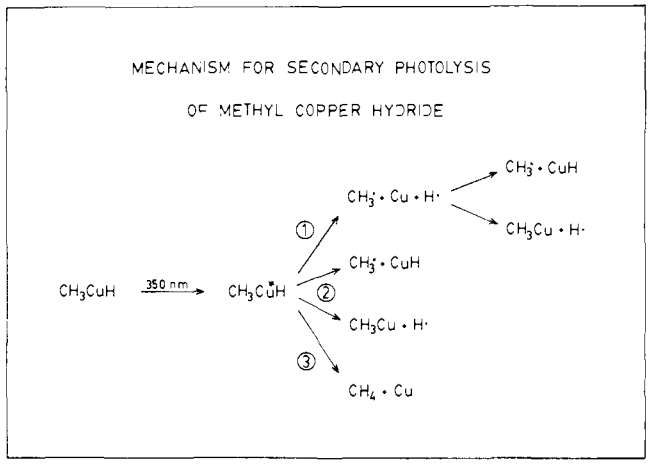

Figure 12. Possible mechanistic pathways for 350-nm photolysis of CH_3CuH in methane at 12 K. (1) Total fragmentation, (2) partial fragmentation, and (3) reductive elimination.

distribution pattern during 305–325-nm photolysis is the same as that involved during 350-nm photolysis.

Infrared studies of partially photolyzed Cu atoms in methane (315 nm, 30 min) before and after 350-nm photolysis were carried out and are presented in Figure 11. The absence of peaks associated with CH_3CuH (1697 and 1011 cm^{-1}) as well as significant growth of bands associated with CuH, CH_3Cu, and CH_3 can be clearly seen after 350-nm photolysis. In all cases, the growth of CuH was much greater than that of CH_3Cu, which correlates with the preferred growth of methyl radicals relative to hydrogen atoms as observed in the ESR spectra. Also note that bands at 433, 414, and 351 cm^{-1} remain after 350-nm photolysis, confirming their assignment to CH_3Cu rather than CH_3CuH.

It is clear from the above results that several fragmentation pathways are active in the 350-nm photolysis of CH_3CuH. As with 305–325-nm Cu atom photolysis, every possible fragment that would result from any combination of bond cleavages at the copper center can be seen to increase in concentration during the photolysis. The three most likely fragmentation pathways for this process are illustrated in Figure 12. These are (1) total fragmentation to form Cu, CH_3, and H, (2) partial fragmentation to give CuH and CH_3 or CH_3Cu and H, and (3) reductive elimination to yield copper atoms and methane. None of these mechanisms alone can account for all the observed products, so

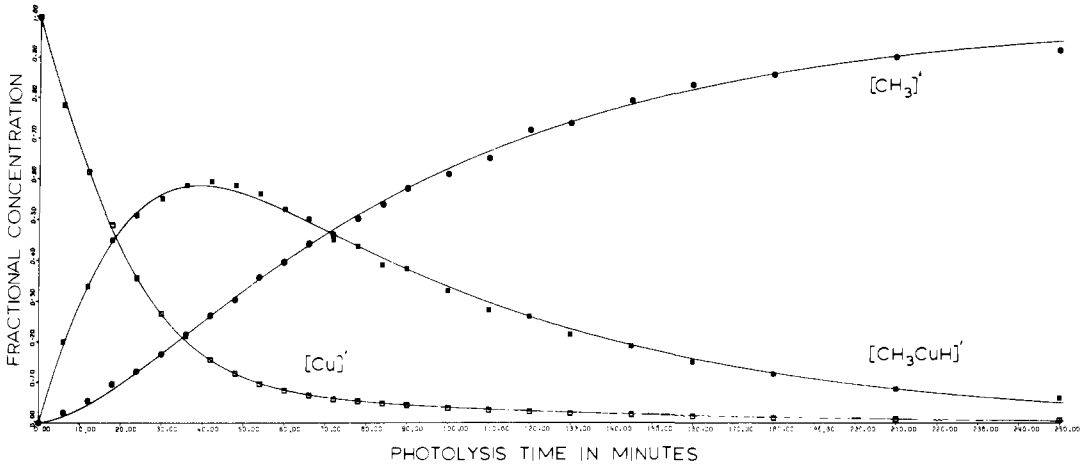

Figure 13. Growth and decay patterns for Cu, CH_3 and CH_3CuH during 305-nm photolysis of a Cu/CH_4 matrix, based upon ESR peak height. Plotted is the normalized concentration of each species vs. photolysis time t at 305 nm. Solid lines are theoretically generated growth and decay curves.

it is clear that more than one pathway is active. The partial fragmentation route is probably predominant since neither of the other pathways leads to significant production of CuH and CH_3Cu. As suggested in Figure 12, there exists the possibility that CuH and CH_3Cu could be formed by a recombination process following a total fragmentation, brought about as a result of the so-called matrix cage effect. Such a process would, however, favor the formation of CH_3Cu and H atoms due to the greater size and mass of methyl radicals with respect to hydrogen atoms. Since CH_3 + CuH is found to be favored by about 80:1, we conclude that this pathway is not a significant route to partially fragmented products. At the same time, the total fragmentation route is considered to be an unlikely source of copper atoms, since such a decomposition is relatively rare with respect to partial fragmentation reactions. In light of the fact that reductive elimination has been proposed as the sole route for photoinduced decomposition of CH_3FeH[10] and CH_3MnH,[11] it is likely that such a process is responsible for the production of copper atoms in the Cu/CH_4 system. (Note that if one accepts a linear structure for the ground electronic state of CH_3CuH, one would have to invoke bending of the molecule in the electronically excited state responsible for a concerted reductive-elimination pathway.) The favored mechanism for photoinduced decomposition of CH_3CuH is therefore considered to be a combination of partial fragmentation and reductive elimination, the former being the predominant pathway.

ESR Photochemical Behavior Simulation. The question now remains as to whether the fragments formed during primary photolysis of copper atoms at 305–325 nm arise solely from tail-end photolysis of CH_3CuH, from a combination of tail-end photolysis and hydrogen abstraction to form CuH + CH_3 or formation of CH_3CuH in an unbound or dissociative excited state immediately following C–H bond cleavage. As mentioned above, the ratio of CH_3/H present in the ESR spectra of matrices containing large amounts of CH_3CuH did not change significantly after 350-nm photolysis although significant growth of both did occur. It was felt that if all fragments resulted from secondary photolysis, the ratio of CH_3/H would remain constant during the entire 305–325-nm photolysis, both before and after copper atom depletion. Conversely, if the fragments arise from both primary and secondary photolysis, the ratio of CH_3/H should vary as the relative concentrations of Cu atoms and CH_3CuH change. In light of the fact that the concentration of CH_3 and H continues to increase until well after the complete disappearance of copper atoms and that the relative ratio of CH_3 to H does not change significantly after the copper atoms are depleted, we felt that the reaction products arose from a fragmentation mechanism involving a single source, namely, secondary photolysis of CH_3CuH by tail-end absorption.

In order to better establish the validity of the mechanism proposed above, computer simulation of the growth and decay of Cu, CH_3CuH, and CH_3 ESR absorption was undertaken. A numerical integration technique was devised whereby the relative concentration of each species was calculated at closely spaced intervals by means of a concentration-dependent rate-of-change expression. Optimization of the growth and decay curves generated from these expressions with respect to the experimental data was then performed, giving rise to theoretical curves which are in excellent agreement with the observed data (Figure 13).

The type of expression used was derived from a simple equation for the rate of change in the concentration of a photochemically active species during photolysis

$$-\mathrm{d}[X]/\mathrm{d}t = \phi_{xy} I_0 (1 - \exp(-\epsilon_\lambda l[X])) \quad (1)$$

where ϕ_{xy} represents the quantum yield for conversion of species x to y, I_0 and ϵ_λ the photon flux and extinction coefficient at the photolysis wavelength, and l the sample thickness. This equation reflects the dependence of the photolysis rate on the photon flux according to the Beer–Lambert law as well as on the efficiency of photochemical conversion. It assumes a photolysis bandwidth which is small with respect to the absorption bandwidth of the active species (ϵ_λ is constant over the range of photolysis bandwidth) as well as a uniform concentration of active species and constant photon flux over the sample surface. Such conditions have been met in this study by means of a narrow photolysis bandwidth (5 nm fwhm), a diffused photolysis source, and small sample area.

Although in principle equations of the form of eq 1 could be used to simulate the photochemical behavior observed in the Cu/CH_4 system, in practice it is very difficult to measure the absolute concentration of species of interest in the matrix. It is, however, possible to accurately measure species concentration relative to either an initial or final value by means of ESR signal peak-height comparison. Thus, at any time t, the relative concentration of copper atoms, [Cu]′, is equal to the ratio of any copper atom signal peak height at time t with respect to the initial height of that same peak (eq 2). This expression is valid only

$$[Cu]' = [Cu]_t/[Cu]_0 \quad (2)$$

if the line shape of the peak in question does not vary significantly with the free-radical composition of the matrix, which changes during the course of the reaction. We have been unable to detect any such change and therefore feel that eq 2 is a reasonable means of measuring [Cu]′. In the same way, $[CH_3]'$ can be measured with respect to the methyl signal peak height after complete photolysis. If the branching ratio for all products remains the same during the reaction, $[CH_3]'$ has special significance in that it represents the extent of final product formation where

$$[CH_3]' = [CuH]' = [CH_3Cu]' = [H]' \quad (3)$$

As the growth behavior of all final products, whether observed by ESR or IR, gives rise to superimposable "S"-shaped growth curves, we feel that eq 3 is valid for this system. The measurement of $[CH_3CuH]'$ is slightly more complicated in that the theoretical

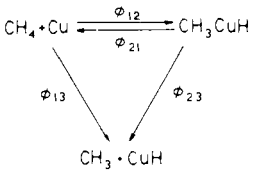

Figure 14. Reaction sequence used in the simulation of the growth and decay behavior of ESR absorptions due to Cu, CH_3CuH, and CH_3.

maximum yield for this species is never attained due to its concomitant fragmentation during photolysis. It is therefore necessary to use the maximum peak height observed as the point of reference and include a normalization factor Q wherever $[CH_3CuH]'$ is used, where Q is determined experimentally by means of a simple copper atom mass balance equation

$$[Cu]' + [CH_3]' + Q[CH_3CuH]' = 1 \quad (4)$$

With the above in mind, we may modify eq 1 by substituting the normalized concentration $[X]'$ for the absolute concentration to obtain

$$-d[X]'/dt = F_{xy}(1 - \exp(-a[X]')) \quad (5)$$

where $F_{xy} = \phi_{xy} I_0/[X]_0$ and $a = \epsilon_\lambda l[X]_0$.

Using the relationship in eq 5, we may mathematically describe the series of simultaneous reactions observed in the Cu/CH_4 system. Figure 14 illustrates the reaction network utilized in the computer simulation. Note the absence of routes from final products to either CH_3CuH or copper atoms, as no evidence for such a pathway was found. A direct route from copper atoms to final products was included and was found to significantly improve the simulation of the CH_3 growth curve during the initial stages of the reaction (i.e., when [Cu] is high but $[CH_3CuH]$ is low). The rate of change expressions which mathematically describe the relationship depicted in Figure 14 are given in eq 6–8.

$$-d[Cu]'/dt = (F_{12} + F_{13})(1 - \exp(-a[Cu]')) - F_{21}(1 - \exp(-bQ[CH_3CuH]')) \quad (6)$$

$$d[CH_3CuH]'/dt = F_{12}(1 - \exp(-a[Cu]')) - (F_{21} + F_{23}) \times (1 - \exp(-bQ[CH_3CuH]')) \quad (7)$$

$$d[CH_3]'/dt = F_{13}(1 - \exp(-a[Cu]')) + F_{23}(1 - \exp(-bQ[CH_3CuH]')) \quad (8)$$

These equations were used to generate theoretical growth and decay curves such as those in Figure 13, by means of numerical integration. Parameters were adjusted to give the best agreement with experimental data by using a multiparameter least-squares fitting routine.[33] In all cases studied, excellent agreement was obtained between theoretical curves and experimental data. Typical root mean square errors were in the range 0.005–0.010 (i.e., 0.5–1% difference) for data points ranging from 0 to 1. Unfortunately, a number of solutions giving practically identical error could be obtained for any one set of data, indicating that the restrictions on the theoretical parameters are not sufficient to find a unique solution. In spite of this, the excellent agreement obtained indicates that the proposed mechanism for reaction is consistent with the experimentally observed behavior. The growth of methyl radicals is found to depend almost entirely upon the concentration of CH_3CuH, which supports the proposal that most of the final products arise as a result of secondary photolysis of CH_3CuH. In all cases, the best fit included a small reproducible contribution to methyl growth from a pathway leading directly (one step) from copper atoms to final products ($F_{13}/F_{12} = \phi_{13}/\phi_{12} = 0.03$–$0.10$). This suggests the existence of either a minor abstraction route ($Cu(^2P) + CH_4 \rightarrow CuH + CH_3$) or a small amount of fragmentation occurring immediately following the formation of CH_3CuH ($CH_3CuH^* \rightarrow CH_3 + CuH$), as suggested in Figure 9 and discussed above. However, as the magnitude of this contribution is small, we cannot eliminate the possibility that the effect is an experimental or computational artifact.

(33) Powell, M. J. D. Subroutine VA05AD, AERE Subroutine Library, Harwell, Didcot, Oxon., U.K.

There still remains the fundamental question as to whether CH_3CuH originates from a straightforward insertion reaction or an abstraction/recombination process. Unfortunately, in a study which does not probe the dynamics of the system, one cannot distinguish between these two possibilities, since the net photochemical result of both processes is the same.

Structure of Methylcopper Hydride. The exact structure of methylcopper hydride, CH_3CuH, has not as yet been determined from our studies of its spectra in methane matrices. It is most unfortunate that a critical region of the ESR spectra of CH_3CuH is rather significantly (and unavoidably) obscured through overlap with strong absorbances due to secondary product methyl radicals. However, as mentioned above, that portion of the spectrum which is observed is characteristic of an axial complex, which limits the geometry to that of a linear molecule, most likely of C_{3v} symmetry.

Ab initio SCF calculations at the RHF level have been carried out on CH_3CuH by Poirier et al.[34] The calculated ground-state geometry for this molecule was found to be somewhat unusual, being best described as a methyl radical linked through an abnormally long Cu–C bond to a closed-shell CuH fragment.[35] Total energy calculations showed CH_3CuH to be thermodynamically more stable than both $Cu(^2P) + CH_4$ and the fragment combinations $CH_3 + CuH$ and $CH_3Cu + H$. The calculations also indicate that the combination $CH_3 + CuH$ is lower in energy than $CH_3Cu + H$, which agrees with the observed distribution of products being in favor of the former.

There are, however, a number of observations which lead us to conclude that CH_3CuH is best described as a copper formal oxidation state II compound, having a linear C_{3v} structure and essentially normal Cu–C and Cu–H bonds. Primary evidence for the above proposal is found in the ESR spectra of CH_3CuH, in which the dominant hyperfine interaction is due to coupling of the unpaired electron with the copper nucleus. The magnitude of the copper hyperfine strongly suggests that the electron resides in a mainly d-type orbital. Superhyperfine coupling to ^1H, ^2H, and ^{13}C nuclei indicates that the molecular orbital containing the unpaired electron is also comprised of contributions from the hydrogen 1s and carbon 2s and 2p orbitals. It is therefore clear that the spectrum is that of an electron located in a three-center, delocalized molecular orbital centered on the copper nucleus and not that of a methyl radical associated with CuH.

With the above in mind, it is important to note that there are two observations which indicate that the copper–carbon bond is weaker than that expected for a typical methyl-bearing transition-metal complex. Firstly, the absence of low-frequency modes associated with CH_3CuH suggests that the Cu–C bond is weak and that the Cu–C stretching mode occurs below the 250-cm^{-1} low-frequency limit of the PE 180 spectrometer. Secondly, the symmetric deformation of the methyl group is about 100 cm^{-1} below the range commonly associated with such vibrational modes,[36] again implying a weaker than normal Cu–C bond.

Covalent Chemical Interactions for the Insertion Pathway. The initial insertion of ^2P Cu atoms into CH_4 in the condensed phase can be considered as a highly efficient process of chemical quenching of the excited state, similar to that involved in the quenching of the first $^1P_1$ excited state of gaseous group 2 and 12 metal atoms by H_2 and alkanes.[37-40] In this case, the quenching

(34) Poirier, R. A.; Ozin, G. A.; McIntosh, D. F.; Csizmadia, I. G. *Chem. Phys. Lett.* **1982**, *101*, 221–228.

(35) Such a structure in which the methyl radical is weakly bonded to a slightly perturbed diatomic molecule has been observed in matrix isolation studies of the thermal reaction of alkali metal atoms with methyl halides (Tan, L. Y.; Pimentel, G. C. *J. Chem. Phys.* **1968**, *48*, 5202–5204). Although these studies were carried out in an attempt to probe isolated methyl radicals, the IR spectra obtained were different from those of methyl radicals generated by vacuum-UV photolysis of methane in argon (25), and could only be rationalized by invoking a weak interaction between CH_3 and the alkali halide. It is likely, however, that when UHF/CI calculations are done on CH_3CuH, the unusually long Cu–C bond will not be found, since effects of this type are known to arise in RHF geometry calculations of open-shell molecules.

(36) Maslowski, E. "Vibrational Spectra of Organometallic Compounds"; Wiley: New York, 1976; p 3.

(37) Callear, A. B.; McGurk, J. C. *J. Chem. Soc., Faraday Trans. 2* **1973**.

(38) Breckenridge, W. H.; Renlund, A. M. *J. Phys. Chem.* **1978**, *82*, 1484.

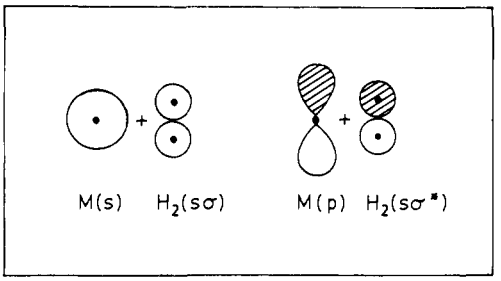

Figure 15. Covalent interactions which are expected to be important in the initial stages of the quenching of the $^1P_1$ excited state of gaseous group 2 and 12 metal atoms by hydrogen. These types of interactions are also expected to be involved in the reaction of ^2P copper atoms with methane at 12 K.

is thought to occur via a direct covalent chemical interaction between the excited atom and the quenching molecule. Callear et al.[37] and Breckenridge et al.[38,39] have considered reaction pathways involving side-on attack of molecular hydrogen or of the C–H bond of an alkane by the excited-state metal atom. The covalent chemical interactions which are expected to be important in the initial stages of such a reaction are illustrated for H_2 in Figure 15. The $^1P_1$ excited state of a group 2 or 12 metal atom is derived from a ns^1np^1 configuration, and hence the singly occupied ns and np metal atomic orbitals are available for bonding with the $s\sigma$-bonding and $s\sigma^*$-antibonding molecular orbitals of H_2, respectively. Since the $s\sigma$ level of H_2 is doubly occupied, it is expected that the metal(s)–$H_2(s\sigma)$ bonding interaction would lead to a transfer of electron density from the bonding molecular orbital of H_2 to the metal atom. On the other hand, the $s\sigma^*$ level of H_2 is unoccupied, and hence the interaction involving the singly occupied p orbital of the metal atom results in a transfer of charge from the metal atom to the antibonding molecular orbital of H_2. Both of these metal–H_2 bonding interactions lead to a weakening of the H–H bond. The case of a C–H bond of an alkane molecule can be considered to be analogous, as the nodal properties of the C–H bonding and antibonding orbitals are similar to those of the corresponding orbitals of H_2. Note also that each of these interactions tends to reinforce the other in a "synergistic" manner that is likely to increase dramatically along the reaction coordinate.

It is expected that this type of interaction is also present in the case of copper atoms reacting with H_2[13] or CH_4. The ^2P excited state involved in the reaction is derived from a $4s^04p^1$ configuration. As with the group 2 and 12 atoms, one would expect the same type of charge-transfer processes between the quenching molecule and metal atom but possibly with a more pronounced donation from the C–H σ bond to the Cu 4s, since the latter is unoccupied. The ^2D state of atomic Cu, having a $3d^94s^2$ configuration, is not expected to be reactive toward CH_4 by a charge-transfer mechanism of the above type.

Conclusion. The overall reaction mechanism for the photoactivation of methane by copper atoms can be summed up in the following manner. Initial $^2P \leftarrow {}^2S$ excitation of copper atoms at 305–325 nm gives rise to an efficient insertion of Cu atoms into the C–H bond of methane to form CH_3CuH. This intermediate is subsequently photolyzed by tail-end absorption in the broad band centered at 350 nm to form mainly CH_3 and CuH. Secondary photolysis of CH_3CuH at 350 nm gives rise to CH_3, CuH, Cu atoms, CH_3Cu, and H atoms, by a combination of partial fragmentation (75%) and reductive elimination (25%) pathways. The formation of CH_3 and CuH is favored over that of CH_3Cu and H by a factor of about 80:1 during photolysis at both 305–325 and 350 nm. Thermal annealing of a matrix containing these fragments results in the reformation of CH_3CuH from CH_3 and CuH or CH_3Cu and H. The question as to whether CH_3CuH originates from a direct insertion step or by way of an abstraction/recombination has yet to be resolved.

There are other systems under active study in our laboratory which differ in varying degrees from the metal atom photochemical reactions described in this paper. It is becoming clear that each metal atom will have its own unique photochemistry and possibly state selective reactivity patterns. The challenge remains to unravel the many factors which contribute to the radiative and nonradiative relaxation processes of electronically excited transition-metal atoms with a range of small molecules.

Acknowledgment. The financial assistance of the Natural Sciences and Engineering Research Council of Canada's Operating and Strategic Grants program are greatly appreciated. We would like to acknowledge the technical assistance of Dr. Douglas McIntosh with the normal coordinate analysis of CH_3Cu and Dr. Saba Mattar with ESR studies. Helpful discussion with Prof. William H. Breckenridge and John G. McCaffrey is gratefully acknowledged. J.M.P. wishes to thank the NSERC for a graduate research scholarship. S.A.M. acknowledges the NSERC and Noranda for graduate scholarships during the earlier and latter stages of his work. J.G.-P. thanks the Instituto Mexicano del Petrolio for financial support of his research during his leave of absence at the University of Toronto.

Registry No. CH_3CuH, 88778-41-0; $CuCH_3$, 1184553-8; CuH, 13517-00-5; Cu, 7440-50-8; CH_4, 74-82-8; CH_3·, 2229-07-4.

(39) Breckenridge, W. H.; Renlund, A. M. *J. Phys. Chem.* **1979**, *83*, 1145.
(40) Adams, N.; Breckenridge, W. H.; Simons, J. *Chem. Phys.* **1981**, *56*, 327.